CNRS
Centre National de la Recherche Scientifique

INFN
Instituto Nazionale di Fisica Nucleare

Timing calibration during VSR1

A. Masserot, B. Mours, L. Rolland

VIR-028B-08

June 23, 2008

VIRGO * A joint CNRS-INFN Project
Project office: Traversa H di via Macerata - I-56021 S. Stefano a Macerata, Cascina (PI)
Secretariat: Telephone (39) 50 752 521 – Fax (39) 50 752 550 – e-mail virgo@pisa.infn.it

Contents

1 Introduction

In order to make multi-detector coincidences, the absolute time of the detector data must be known. After a brief overview of the timing system [1], the absolute timing of the Virgo data is estimated.

In order to get a good accuracy of the h(t) reconstruction, the delays from the longitudinal correction signals applied to the mirror and marionnette actuators and the dark fringe must be set within a few μs. Delays of the order of 450 μs have been measured through the actuator calibration main stream [2] from the control signal Sc_ * _zCorr to the dark fringe signal Pr_B1_ACp. In this note, we consider the processing of the signals in order to explain such delays and estimate possible systematic errors.

Finally, some checks about the stability of the Virgo timing system are described.

2 Virgo timing system overview

The Virgo timing system is based on a master timing system controlled by GPS. Its roles are to give the rythm of the control loops and to give the time stamps to the acquisition system (DAQ).

The GPS receiver delivers a 5 MHz signal to the master timing board. The master timing board then builds four signals which are then distributed through optical fibers to the different buildings in order to control loop frequencies and to give the time to the acquisition system:

- a *fast clock* signal (2.5 MHz),
- a sampling signal at 20 kHz to sample the rapid signals,
- a *frame signal* at 1 Hz to define the frame limits,
- a signal at 1/32768 Hz (or triggered by the user) to define the "run" limits. It is used to synchronize the frame numbers.

A quartz oscillator is set on the GPS board, with a relative stability of $\sim 10^{-6}$. However, the frequency of this oscillator is enslaved on the GPS time: corrections of the time and of the frequency are applied as function of the GPS system information. Deviations of the output time with the GPS time are less than 1 μs.

A few microseconds $t_1 \sim 3\,\mu$s delay is expected between the clock from the GPS receiver and the *frame* signal from the timing system. To monitor it, the 1 Hz *frame* signal is sent back to the GPS receiver in order to measure its delay from the beginning of the last second in the GPS. This delay is stored in the Virgo data in the channel TiM_GTimeN (in ns). It can change when the timing system is restarted or when the GPS encounter problems (for example, a temporary loss of satellites).

The four output signals from the master timing system are delivered to the timing distribution boards of the different buildings. They are first converted to optical signals and sent through silica optical fibers with refraction index of the order of 1.5. In order to have the same propagation delays for all buildings, all the optical fibers have the same length ($3350 \pm 100\,\mathrm{m}$). The expected propagation delay is of the order of $t_p = 16.8 \pm 1\,\mu\mathrm{s}$. The optical signals are then converted to electrical signals, distributed from the timing distribution boards to the user crates and used to control the rate of the different processes.

From every building, the local distribution boards send back the 20 kHz and 1 Hz clock signals to the control part of the master timing board. The signals are compared to the clock of a second GPS receiver. The total delay between the propagated clock signals and the initial clock signals from the master timing board is stored in four channels TiM_rtt$(1, 2, 3, 4)$ (in ns) corresponding to the four buildings returned signals. The four delays are expected to be the same and of the order of $t_2 = 2 \times t_p = 33.6 \pm 2\,\mu\mathrm{s}$.

3 Absolute timing of the Virgo data

Specific data have been taken in April 2008 in order to check our understanding of the timing delays and estimate the systematic error on the absolute timing of the Virgo data.

The absolute timing during VSR1 is then estimated.

3.1 Estimation of the systematic error

Measurements to characterize the Virgo absolute timing have been performed during the night from 7th to 8th April 2008. They are analysed in the following paragraphs.

3.1.1 Estimation of the propagation time of the clock signals

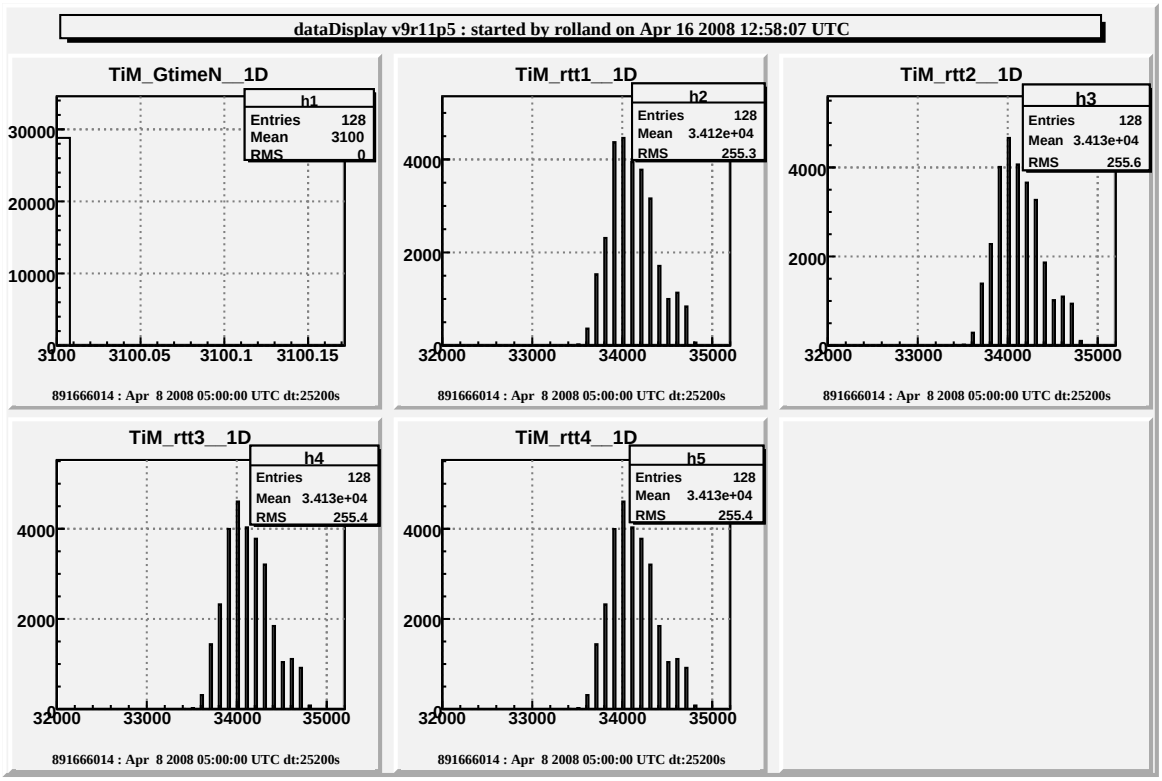

Figure 1: ***Distribution of the timing monitoring signals*** *during the night from 7th to 8th April 2008. The unit of the channels are ns.*

On April 8th 2008, the delay between the GPS receiver and the clocks from the master timing board, measured in the channel TiM_GTimeN, was $t_1 = 3.1\,\mu$s (figure 1). The propagation delay from the master timing clock and the second GPS receiver, measured though the channels TiM_rtt$(1, 2, 3, 4)$ was $t_2 = 34.1\,\mu$s, with a RMS of 255 ns. From this measurements, the

propagation time from the master timing board to the timing distribution boards is estimated to $t_p = 17.1\,\mu$s. This is in agreement with the expected propagation time delay within $0.3\,\mu$s. For this night, the expected delay of the Virgo data related to the GPS time is thus estimated to be $t_1 + t_p = 20.2\,\mu$s.

3.1.2 Estimation of the frame time delay from the GPS time

The 1 PPS signal from the master timing GPS receiver has been sent to an ADC of the dark fringe photodiode readout in the central building and stored in the data through the DAQ. This allows to measured the delay between the rising-edge of the 1 PPS signal, giving the absolute beginning of a second, and the first sample of the frame. The frames are defined such that the first sample is at a time with an integer number of seconds. This delay thus gives the absolute delay of the Virgo data.

In practice, the 1 PPS output is a 500 ms rectangular signal. The rising edge of the signal is detected by a flip-flop which rapidly triggers the integration of a reference signal. The signal is integrated up to a given value and the output of the integrator is reset to 0. The ramp is digitized through a 4-channels ADC (without anti-alias filter) and stored into the frames. An example of such a signal[1] is shown in the figure 2(a). The time of the rising-edge of the GPS signal is given by the time of the beginning of the ramp. This one can be adjusted fitting a line on the whole ramp and finding when it crosses the pedestal level[2].

Such data have been taken during the night from 7th to 8th April 2008. Every ramps (stored in the channel Pr_TiPulse) have been adjusted by a line. The offset between the initial time of the ramp t_0, giving the time of the GPS pulse, and the time of the frame starting just after have been calculated. Its distribution is given in the figure 2(b). An average offset of $23.2\,\mu$s with RMS of $1.2\,\mu$s is found. The dispersion of the measurements is probably due to the bad estimation of the pedestal level which varies under the ramp.

3.1.3 Virgo absolute timing and systematic error

Two measurements of the absolute delay between the Virgo time stored in the frames and the GPS time during the night from 7th to 8th April 2008 give $20.2 \pm 0.3\,\mu$s and $23.2 \pm 1.2\,\mu$s respectively. For multi-detector analysis, the Virgo signals must thus be corrected for a $22\,\mu$s delay. Yet, $\sim 2\,\mu$s systematic errors have to be taken into account in the absolute timing of h(t).

[1] In the plots to be fitted, the ith sample of the FrVect v, with value $v->dataD[i]$ is set at the time of the clock: $v->startX[0] + i \times v->dx[0]$.

[2] There were oscillations of amplitude ~ 0.05 V and frequency around 600 Hz in the data, with discontinuities around the ramp. Thus it was not possible to estimate the pedestal level under the ramp properly. An average value was used.

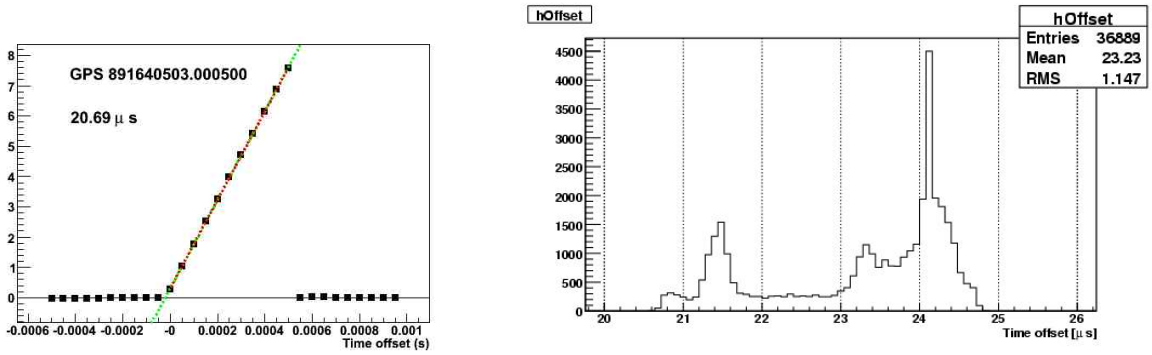

(a) Example of triangular signal.

(b) Absolute time delay distribution.

Figure 2: ***Example of triangular signal built from the GPS 1 PPS signal.***

3.2 Absolute timing during VSR1

The first method described above to measure the propagation time of the clock signals can be applied on the VSR1 data since the timing signals were monitored.

The timing monitoring signals as function of time during VSR1 are shown on the figure 3. The delay measured by TiM_GTimeN changed on August 3rd 2007, around 14h18m42s UTC. It was $t_1 = 2.7\,\mu$s up to GPS 870185936, and then $t_1 = 2.3\,\mu$s from GPS 870185936. The $0.4\,\mu$s variation is within the timing systematic errors and can be neglected in the h(t) reconstruction. However, it must be added to the systematic errors.

The return-time monitoring signals TiM_rtt$(1, 2, 3, 4)$ were constant during VSR1, with an average of $t_2 = 34.15\,\mu$s and a RMS of $0.26\,\mu$s.

From these measurements, the absolute delay during VSR1 is $2.7 + 17.1 = 19.8\,\mu$s. It is compatible with the measurements described in previous section.

The h(t) reconstructed using the VSR1 data must thus be corrected for a $21\,\mu$s **delay. The systematic errors on the absolute timing of h(t) are estimated to** $2\,\mu$s**.**

4 Calibration of the dark fringe sensing

In the h-reconstruction, the signal at high frequency (above a few hundreds Hz) is dominated by the dark fringe signal contribution. It is thus important to calibrate the dark fringe readout electronics and estimate/correct for possible offsets from the absolute timing.

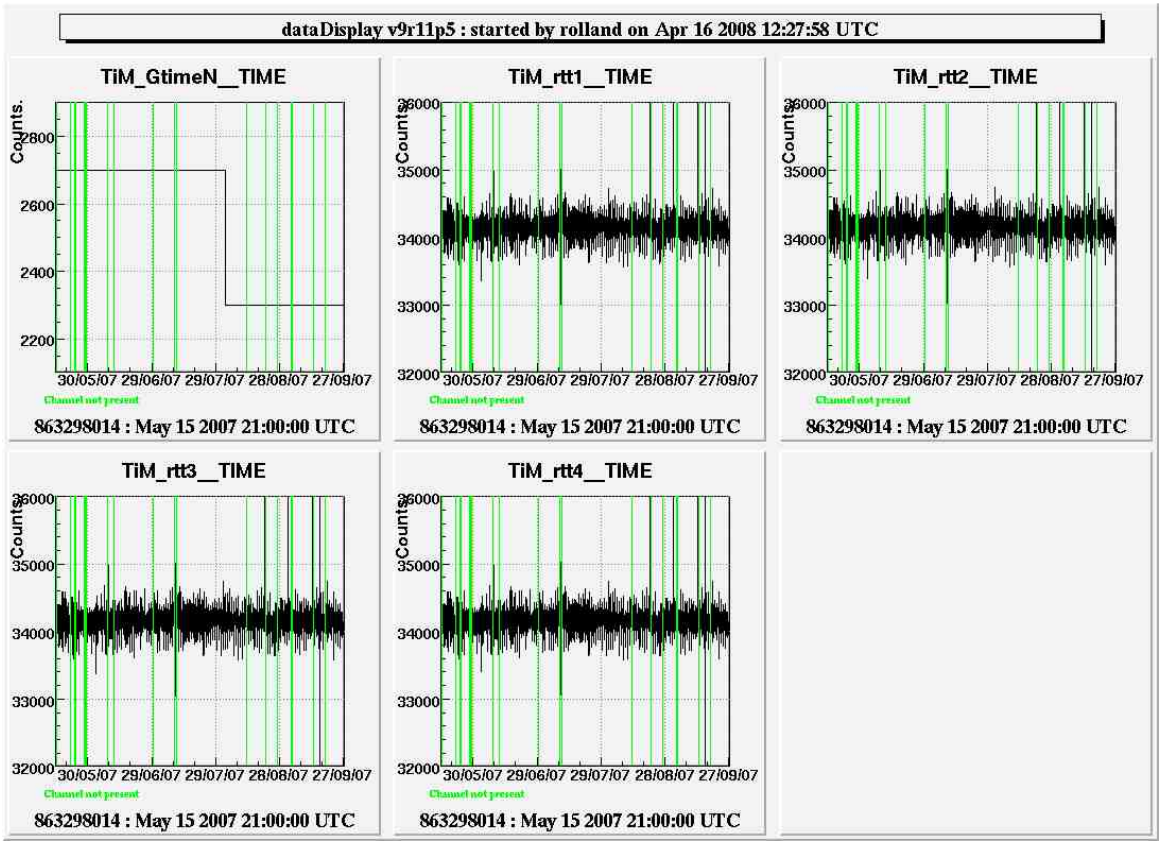

Figure 3: ***Master timing monitoring signals vs time during VSR1.***

From the power inpinging on the photodiodes and the Pr_B1_ACp channel stored in the DAQ, the signal goes through the following path:

- the delay in the dark fringe sensing chain: photodiode, preamplifier, demodulation with a compression filter.
- the ADC readout of the dark fringe sensing, with its anti-alias filter.
- the Pr27 process, with de-compression filter.

The signals from two photodiodes are combined in Pr27 in order to build the dark fringe signal Pr_B1_ACp: Pr_B1_d2_ACp and Pr_B1_d3_ACp.

4.1 Expected delay

The signal processing is shown on the figure 4.

The dark fringe analog power is measured through photodiodes. The output voltage is measured through a pre-amplifier and a demodulation board. It is then filtered through an anti-alias filter which phase below 5 kHz is equivalent to a delay of $70 - 80\,\mu$s. The signal is then read by an 4-channel ADC. (It is one of those that was used to estimate the DAQ timing in section 3.1.2.) The signals from the photodiodes are then mixed and converted into power by the Pr process.

The delay introduced by the photodiode/pre-amplifier/demodulation board should be lower than a few μs. The whitening/de-whitening filters are compensated in Pr27 and should not induce any delay.

The *frame signal* triggers the Pr time stamp. The Pr process has cycles at a rate of 10 kHz. The analog ADC inputs are sampled at 20 kHz and read by Pr which builds the output channel time serie Pr_B1_ACp at 20 kHz, setting the samples such that it does not introduce any delay.

The total delay introduced by the dark fringe sensing is thus the delay of the ADC anti-alias, expected in the range $70 - 80\,\mu$s.

4.2 Stability of the compression filters

The dark fringe channel Pr_B1_ACp is computed using the signals read from two photodiodes, Pr_B1_d2_ACp and Pr_B1_d3_ACp. The B1 compression filters located in the demodulation board have been measured in February 2007[3]. The fitted complex poles and complex zeros (with quality factor of 0.5) are given in the table 1. They have been compensated in Pr27 for

[3]Logbook entry 15067. Noise in injected before the demodulation board. It goes through the demodulation board, the ADC and its anti-alias and Pr27.

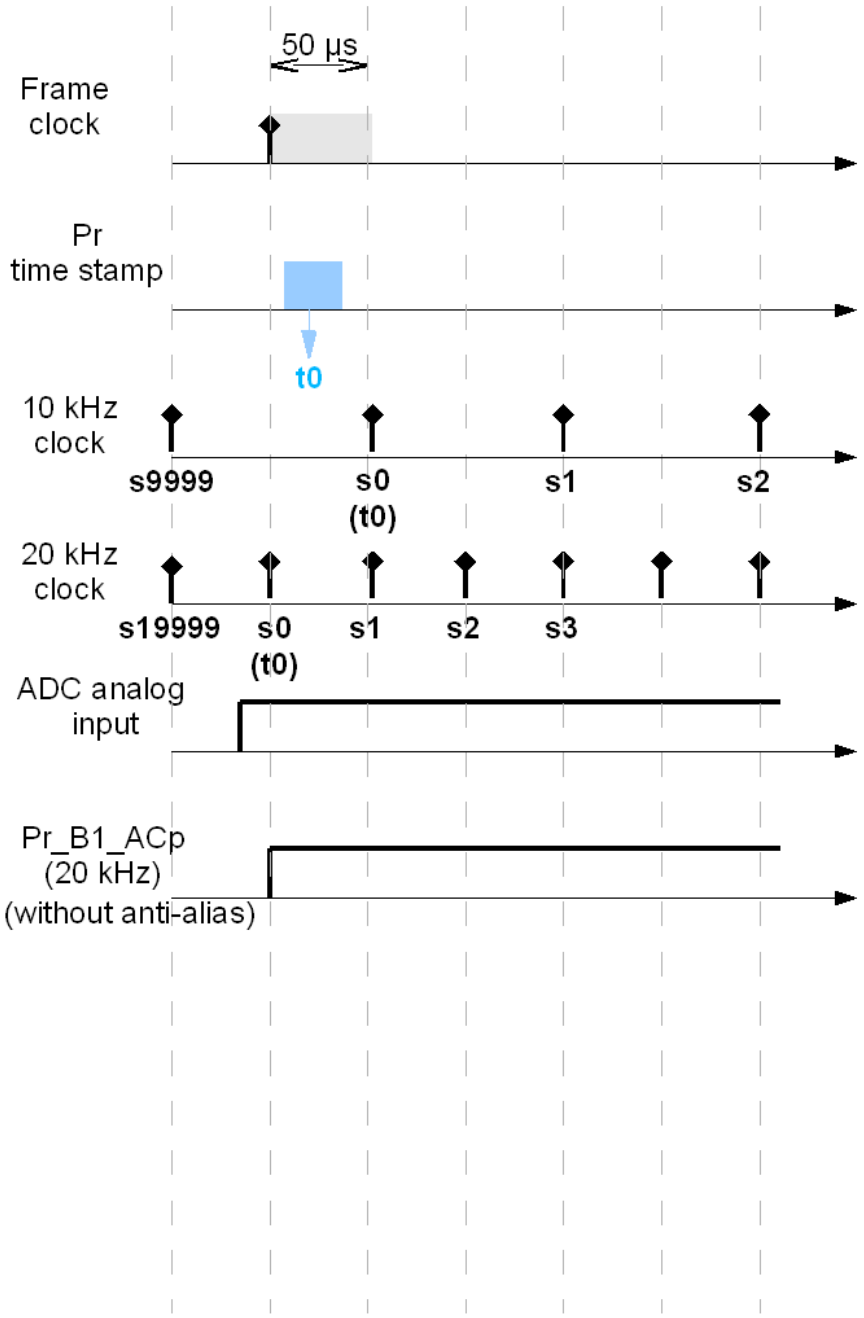

Figure 4: ***Signal processing in the dark fringe sensing part.*** *See text for details.*

every photodiode channels. These values were used during VSR1 for the compensation.

Channel	February 2007		October 2007	
	f_0 (Hz)	f_p (Hz)	f_0 (Hz)	f_p (Hz)
Pr_B1_d2_ACp	22.6	131.6	22.6	131.9
Pr_B1_d3_ACp	26.8	154.7	27.2	157.3

Table 1: ***Compression filter measurements below 1 kHz: double zeros (f_0) and poles (f_p).*** *The online compensation filters set in Pr27 use the values measured in February 2007. The measurements from October 2007 are used to check the stability of the compression filter during VSR1.*

	Pr_B1_d2_ACp	Pr_B1_d3_ACp	Average model
f_N (Hz)	35288 ± 11	20932 ± 2	28110
f_B (Hz)	8636.1 ± 0.2	8726.1 ± 0.2	8681.1
t_d (μs)	-9.964 ± 0.002	-2.319 ± 0.003	-6.1
t_d^{equiv} (μs)	72.8	79.7	76.3

Table 2: ***Fit of the ADC anti-alias filters.*** *Using the Pr27 online compensation filters, the anti-alias filter of both photodiode channels have been fitted with a Butterworth filter (f_B), a notch (f_N) and an additionnal delay (t_d). The overall equivalent delays induced in every channels are also given (t_d^{equiv}). An average model has been derived from the results.*

The compression filters have been measured again in October 2007, during the post-VSR1 calibration shifts[4]. The fitted poles and zeros (using data below 1 kHz) are given in the table 1. They are within 1% of the values used for the compensation in Pr27. This confirms the stability of the compression filter during VSR1.

4.3 Residuals of the compression filter compensation, ADC anti-alias fit

The residuals of the compression filter non-perfect compensation have been estimated comparing the model used in Pr27 to the data. In order to adjust the high frequency part of the transfer function, the anti-alias filter has been fitted with a Butterworth filter and a simple notch.

The residuals of the compression filter non-perfect compensation are shown in the figure 5. The residuals of the compression filter compensation are within $\pm 3\%$ below 6 kHz. It has been

[4] logbook entry 18869

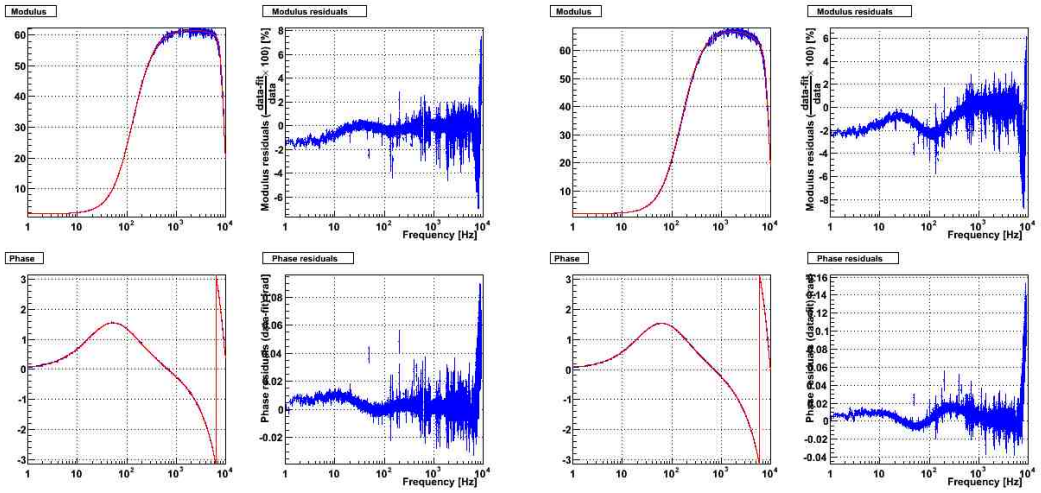

(a) Pr_B1_d2_ACp (b) Pr_B1_d3_ACp

Figure 5: ***Transfer function fits and residuals of the photodiode readout channels.*** *The measured transfer function is plotted in blue. The red curve model is the compensation filter used in Pr27 during VSR1 with an ADC anti-alias filter that have been fitted. The residuals of the fitted model are given.*

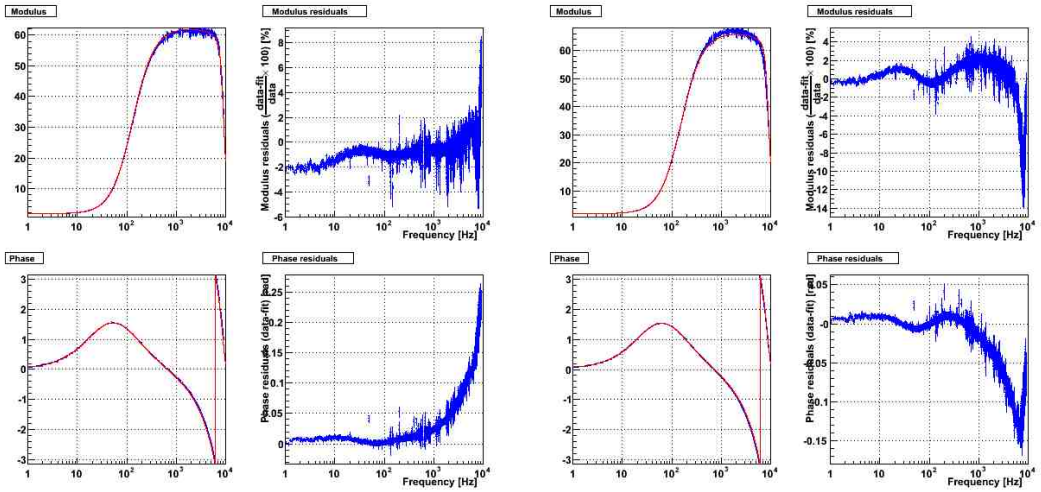

(a) Pr_B1_d2_ACp (b) Pr_B1_d3_ACp

Figure 6: ***Model with an average anti-alias and its residuals.*** *The decompression filters have been set as in Pr27. The averaged anti-alias filter described in the text have been used (Butterworth frequency, notch frequency and delay). Only the gain have been fitted.*

also possible to fit the ADC anti-alias filter shapes up to 10 kHz in the data. The model uses a 7th order Butterworth filter with cut-off frequency f_B and a simple notch at f_N:

$$H(\mathrm{j}f) = \frac{-\left(\left(\frac{f}{f_N}\right)^2 - 1\right)}{\left(1 + \mathrm{j}\frac{f}{f_B}\right)\prod_{k=1}^{3}\left(1 - \left(\frac{f}{f_B}\right)^2 + \mathrm{j}a_k\frac{f}{f_B}\right)} \quad (1)$$

with $a_{1,2,3} = 1.801937736,\ 1.246979604,\ 0.4450418680$.

The transfer functions are fitted from 1 Hz to 10 kHz using the points with coherence higher than 99%. The fitted parameter values are given in the table 2. The residuals are lower than ±10% below 10 kHz. Concerning the delay, below a few kHz,the two fitted filters made of the Butterworth filter, a notch and an additionnal delay are equivalent to a delay of 72.8 and 79.7 μs respectively.

An average anti-alias filter model have been derived. It is given in the table 2. The comparison of the data and the models (online compression filters and average anti-alias filter) as well as the residuals are given in the figure 6. The modulus residuals are still within 3% below 6 kHz but are up to 15% up to 10 kHz. The phase residuals are larger since the delays in the two channels are different but the average model uses the same value for both. Using an average anti-alias filter and delay induces systematic errors of ±4 μs on the combined channel.

4.4 Global fit: compression and anti-alias filters

In order to improve the model for the photodiode readout transfer functions, the data from October 2007 have been fitted with a model including a gain, a delay, a complex zero, a complex pole, a Butterworth filter and a notch (8 free parameters). The fits have been computed from 1 Hz to 10 kHz using the points with a coherence higher than 99%.

The results of the fits of the transfer functions for the channels Pr_B1_d2_ACp and Pr_B1_d3_ACp are given in the table 3. The results and residuals are shown in the figure 7. The residuals are rather flat, lower than 1% in modulus and lower than 0.02 rad in phase below ∼ 6 kHz. It could thus be useful to use such filter in the h-reconstruction and to recombine them afterwards in order to get the dark fringe signal. It would lower the signal distorsion. Also, the timing systematic error of the combined channels would be lower.

4.5 Conclusion

The measurements of the delay induced in the photodiode readout channels are in agreement with the expected values, between 70 and 80 μs. However, a difference of 7 μs is found between the two channels that are combined to compute the dark fringe channel Pr_B1_ACp. It induces ±4 μs systematic errors on the Pr_B1_ACp channel timing. It is possible to reduce this error

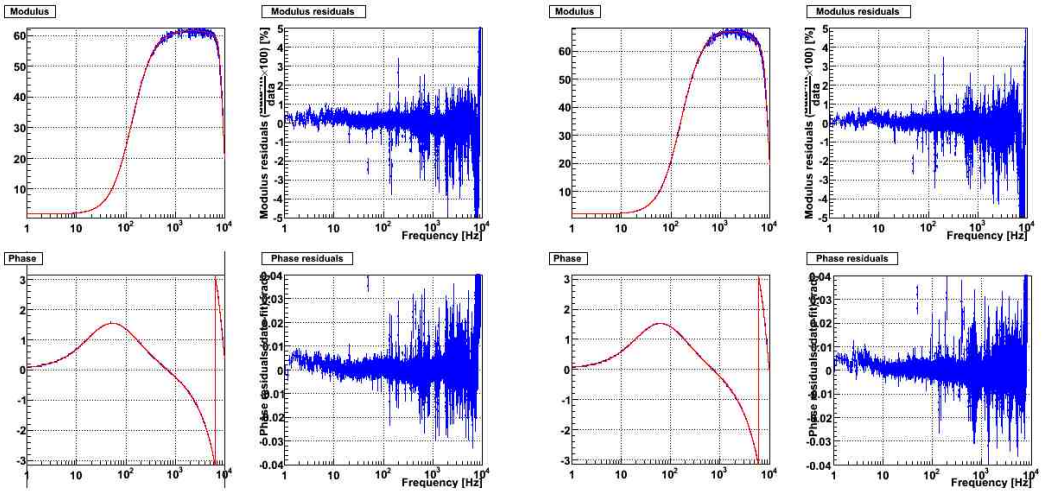

(a) Pr_B1_d2_ACp (b) Pr_B1_d3_ACp

Figure 7: ***Results of the fit of the two dark fringe photodiode readout channel transfer functions*** *with the 8-parameter model. The residuals are also given.*

	Pr_B1_d2_ACp	Pr_B1_d3_ACp
Gain	1.79879 ± 0.00028	1.98613 ± 0.00028
Delay μs	-9.7965 ± 0.0025	-1.7009 ± 0.0027
f_0 (Hz)	22.364 ± 0.002	26.8008 ± 0.0025
Q_0	0.49790 ± 0.00009	0.491723 ± 0.000085
f_p (Hz)	131.39 ± 0.01	157.021 ± 0.015
Q_p	0.49544 ± 0.00004	0.492754 ± 0.000038
f_B (Hz)	8648.35 ± 0.20	8773.09 ± 0.23
f_N (Hz)	34096 ± 11	20077 ± 2.17

Table 3: ***Results of the fit of the two dark fringe photodiode readout channel transfer functions*** *with the 8-parameter model.*

recombining the photodiode signals offline, applying the models including the anti-alias filter fits to each channel.

5 Timing delay from the actuation to the dark fringe

In this section, the details of the signal processing from the mirror actuation input to the dark fringe output are given. The aim is to estimate the expected delay of the signal processing to be compared to the delay found by the calibration main stream.

The signal processing is made of the following pieces:

- the mirror actuation, from Sc_ * _zCorr to the force applied on the mirror. It depends on the mode of the suspension: High Power (HP) or Low Noise (LN).
- the propagation time of the mirror deformation from the magnets to the mirror centre.
- the mechanical response of the pendulum.
- the optical response of the interferometer. It is different between the data in free swinging Michelson configuration and the data in Science Mode.
- the sensing of the dark fringe, from the power on the photodiodes to the Pr_B1_ACp signal.

In the following, the way a digital electronic signal is stored into the DAQ frames is detailed for both the actuation part and the dark fringe sensing. The figures are made around the time of the beginning of a new frame.

The measurement of the transfer functions from actuation to dark fringe from the calibration main stream are done below 1 kHz and without any modelisation of the anti-image and anti-alias filters. Below a few kHz, the TFs of these filters are equivalent to pure delays. The delays induced by the filters are thus taken into account in the following, but not their effects above a few kHz.

5.1 Signal processing in the actuation part

From the channel Sc_ * _zCorr to the force on the mirror, the signal goes through the following path:

- the DSP of the coil actuation,
- the DAC of the coil actuation, with its anti-image filter.
- the coil and serie resistors. They can be modeled with a pole whose value depends on the HP or LN mode of the suspension.

The way the signal goes through this path and is stored in the DAQ is described in order to estimate the expected delay from the recorded channel Sc_ * _zCorr to the force applied on the mirror. The value is then compared to measurements.

5.1.1 Expected delay

The signal processing is shown on the figure 8.

The *frame signal* is a serie of one 50 μs-pulse per second. The DSP signals are sampled with a frequency of 10 kHz. The 10 kHz clock is set such that the *frame* pulse is in-between two 10 kHz-clock pulses. For a 10 kHz time serie, the first sample s_0 contains the value computed between the impulses s_0 and s_1. It is offset from the beginning of the frame by 50 μs.

The ith DSP cycle (i from 1 to 10000) starts and ends with two consecutive 10 kHz clock pulses: s_{i-1} and s_i. In practice, it starts 7 μs after the pulse, but this is not visible in the data stored by the DAQ. During the first cycle (from s_0 to s_1), the DSP gets the input values, makes calculations, writes the output values to the DAC and sends the probed output to the DAQ with the flag of sample s_0. Assuming a DSP input (see figure), its value is thus processes by the DSP when it receives the 10 kHz-pulse s_0. After the calculation, the probed values of $Sc\_ * \_zCorr$ and $Sc\_ * \_zDAC$ (value written in the DAC) are stored in the DAQ in the sample s_0. The DAC readout is triggered by the 10 kHz clock pulses and the corresponding values are thus settled at sample s_1 (this does not take into account the additional delay of the DAC anti-image filter). For frequencies lower than ~ 1 kHz, the phase of the DAC anti-image filter is equivalent to a delay of 180 μs. An additionnal delay of 0.350 μs is expected between the time the DAC is triggered and the time the DAC data are available at the analog output (DAC settling time).

The current flowing in the coil is then filtered by the simple pole[5] made of the coil ($L \sim 3.3 \times 10^{-3}$ H) and the serie resistors ($\sim 50\,\Omega$ in HP mode and $\sim 6\,k\Omega$ in LN mode for the cavity mirrors, $\sim 1\,k\Omega$ in LN mode for the BS mirror). The equivalent delays d_{coil} below the pole frequencies are 66 μs and 0.6 μs (3.3 μs for BS) respectively.

The total delay between the $Sc\_ * \_zCorr$ stored signal and the force applied on a mirror is thus $\sim 330.4 + d_{coil}$ μs. For an end mirror in LN mode, the ~ 331 μs delay is coming from:

- 50 μs between the beginning of the frame and the first 10 kHz sample,
- 100 μs since $Sc\_ * \_zCorr$ is stored by the DAQ in the sample s_{i-1} and the DAC is triggered by the clock pulse s_i,
- 0.350 μs to settle the DAC,
- 180 μs from the DAC anti-image.
- 0.5 μs from the coil and serie resistors.

The expected delay is thus ~ 396 μs for the end mirror actuation in HP mode and ~ 334 μs for the BS mirror actuation.

[5] The pole frequency is defined as $R/(2\pi L)$.

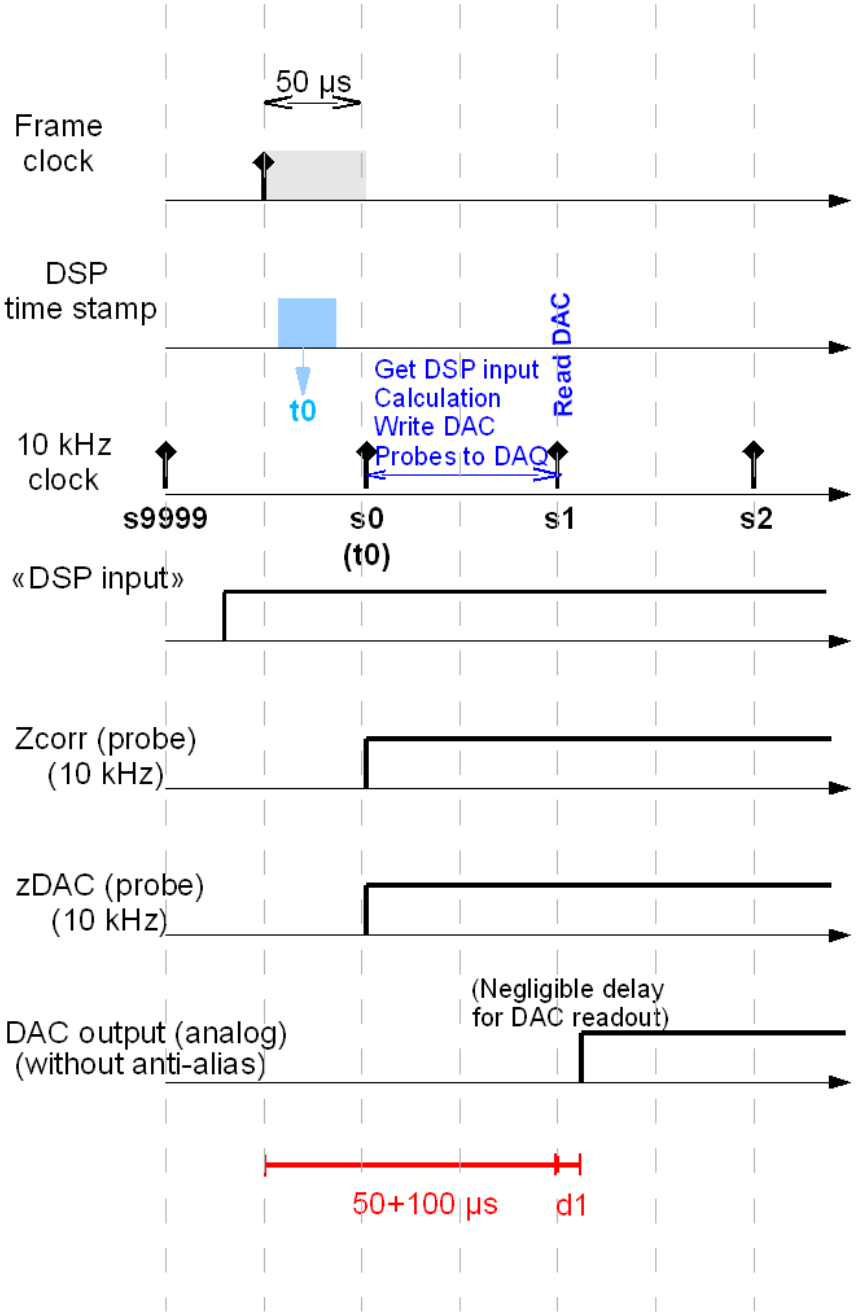

Figure 8: ***Signal processing in the actuation part.*** *See text for details.*

In LN mode, there are emphasis filters in the DSP to compensate the de-emphasis filters set in the coil driver. This should not induce any phase effect between Sc_*_zCorr and the signals after the coil current.

In the calibration stream, the mirror actuation TFs have been corrected for the mechanical response of the pendulum. The phase from the pendulum response should not be taken into accoun in this analysis but should be corrected for in the h-reconstruction.

5.1.2 Measurements of the delay

It is possible to measure the current flowing in the coils using the channels $Ca\_*\_RM\_Coil\{U,D\}$ in order to check the expected delay. This channel is sampled at 20 kHz through a shaping filter with a zero and a pole at 3 and 97 Hz[6]. The sample time is corrected for the 16-channels ADC anti-alias filter delay (~ 1.7 ms) in the DAQ. The 20 kHz sampled channels are not offset from the beginning of the frame. The channels $Ca\_*\_RM\_Coil\{U,D\}$ should thus be in phase with the force applied on the mirror.

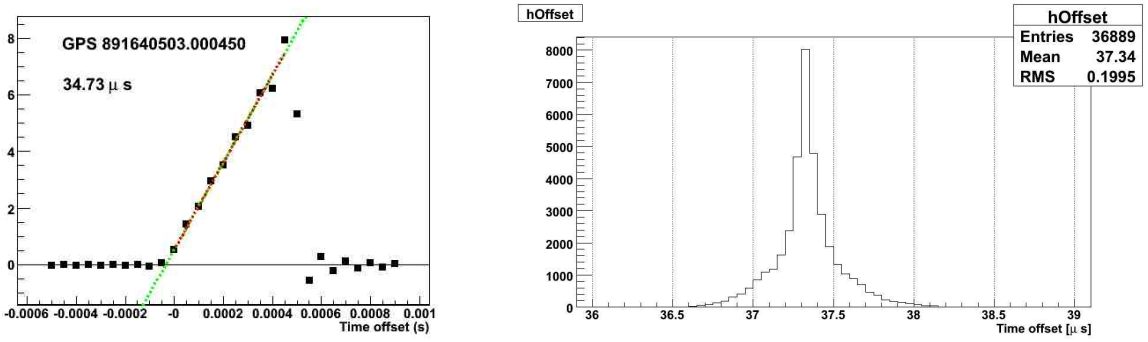

(a) Example of triangular signal in a 16-channel ADC.

(b) Absolute time delay distribution (16-channel ADC).

Figure 9: ***Timing of the 16-channel ADCs.*** *(a) Example of a triangular signal built from the GPS 1 PPS signal and digitized through a 16-channels ADC with its anti-alias filter. The fit used to estimate the absolute GPS time is shown in red (the line is extrapolated in green). (b) Distribution of the offset found between the GPS clock and the sampled signal.*

In practice, the delay of anti-alias filter of the ADC channel is not perfectly corrected in the DAQ. In order to measure the error, the ramp generated from the 1 PPS signal from the GPS receiver has been sent to a 16-channels ADC. This is based on the same method as described in 3.1.2 (p. 5). The triangular signal is filtered by the ADC anti-alias filter, which induces

[6] For the BS channels, an additionnal shaping filter is used with a double zero at 2 Hz and a double pole at 12 Hz

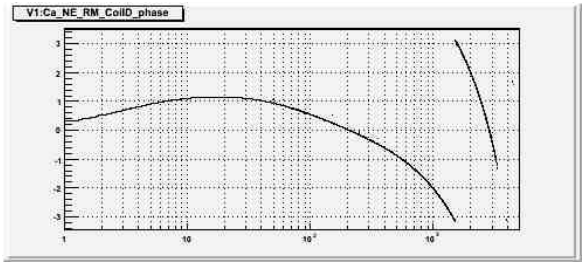

(a) Phase of NE, Coil D

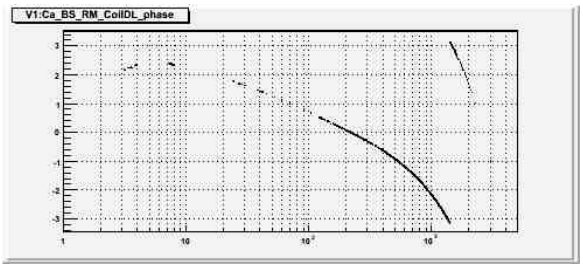

(b) Phase of BS, Coil DL

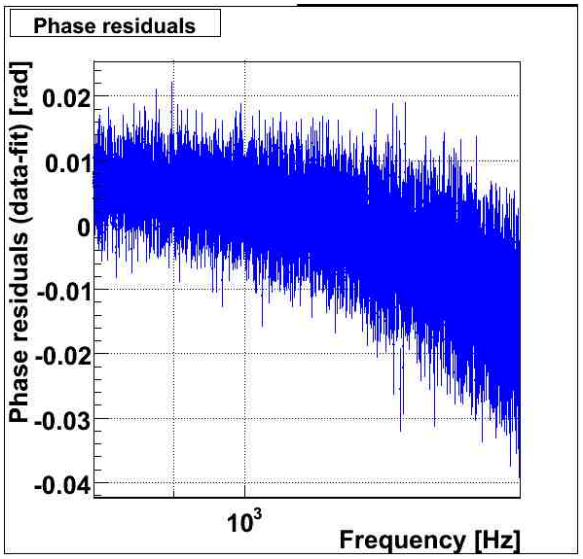

(c) NE coil U.

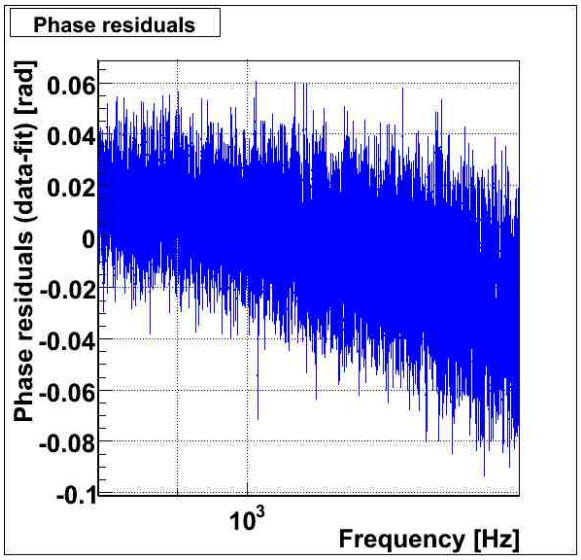

(d) BS Coil DR.

Figure 10: ***Measured phase of the TF*** $Ca\_*\_RM\_Coil*/Sc\_*\_zCorr$ ***and difference from a pure delay model.*** *(a) and (b) Examples of phase (in radians) as function of frequency. The suspensions were in LN mode. Only the points with coherence higher than 99% are shown. (c) and (d) Residuals of the phase compared to a delay from 800 Hz to 1.5 kHz.*

	Tower	Coil	Raw delays $zCorr \rightarrow Ca\_RM\_Coil$			$zCorr \rightarrow$ coil current	
			Minimum (μs)	Maximum (μs)	Average (μs)	Measured (μs)	Expected (μs)
HP mode	NE	CoilU	406	421	411	396	396
	NE	CoilD	393	407	397	382	396
	WE	CoilU	388	417	402	387	396
	WE	CoilD	387	417	404	389	396
	BS	CoilUL	407	425	415	400	396
	BS	CoilUR*	411	430	418	403	396
	BS	CoilDL	411	427	419	404	396
	BS	CoilDR	408	427	416	401	396
LN mode	NE	CoilU	336	345	340	325	331
	NE	CoilD	336	345	340	325	331
	WE	CoilU	338	346	341	326	331
	WE	CoilD	337	345	340	325	331
	BS	CoilUL	318	328	322	307	334
	BS	CoilUR*	327	337	333	318	334
	BS	CoilDL	356	369	362	347	334
	BS	CoilDR	355	370	362	347	334

Table 4: ***Measured and expected delays in the actuation part.*** *The minimum, maximum and average delays measured from the phase of the TFs $Ca\_*\_RM\_Coil*$ over Sc_*_zCorr are given (after correction from the (3-97) Hz readout shaping filter). These raw delays include the delay from the coil current readout in the channels $Ca\_*\_RM\_Coil*$. Only the points with coherence higher than 99% between 500 Hz and 2 kHz were used. *: the phase has been shifted by $-\pi$. There must be a -1 sign in the current readout. The delay errors are of the order of 4 μs. After correction from the current readout delay (15 μs), the derived delays from the longitudinal correction to the current in the coil are given along with their expected values.*

systematic distorsion of the sampled ramp as shown in the figure 9(a). The pedestal of this channel was constant (-0.02 V). The distribution of the absolute time delay of the 16-channels ADC sampled signals to the GPS time is given in the figure 9(b). The delay is of the order of $37.3 \pm 0.20\,\mu$s. $\sim 22\,\mu$s are due to the delay of the Virgo DAQ timing. The additionnal $15\,\mu$s are attributed to the bad compensation of the ADC anti-alias delay in the DAQ. It means that the channels $Ca\_*\_RM\_Coil\{U,D\}$ should thus be delayed by $15\,\mu$s compared to the other stored channels. Note that this error in the delay correction is 1% of the delay induced by the anti-alias filter. Since all the 16-channels ADC have the same digital anti-alias filter and the delay correction used in the DAQ is the same for all channels, the $15\,\mu$s delay should be the same for all channels (in particular for all the $Ca\_*\_RM\_Coil*$ channels).

The transfer functions (TF) of $Ca\_*\_RM\_Coil\{U,D\}$ over Sc_*_zCorr have been measured on VSR1 data from September 28th 2007:

- data in Science Mode, with the suspensions on LN mode (GPS 875001614),
- data in step 4, with the suspensions in HP mode (GPS 875006584).

Examples of measured phase plots are shown in the figure 10. After correction for the the 3-97 Hz shaping filter phase effect[7], the delay is computed for all points with coherence higher than 99% from 1 kHz to 2 kHz. The minimum, maximum and average delays measured for every mirror coil channels are given in the table 4. This delay include the DAQ delay estimated in section 5.1.1 and the addditionnal $15\,\mu$s delay from the 16-channels ADC used in the coil current readout. Examples of the residuals of the measured phase to the model including the shaping filter and a pure delay are shown in the figure 10. The residual errors on the delay are of the order of $4\,\mu$s.

In order to estimate the delay from Sc_*_zCorr to the current in the coil (or the force applied on the mirror), the $14\,\mu$s correction for the readout delay has been applied. The results are given along with the expected values in the table 4.

In HP mode, the measured delays are compatible with the expected ones within $15\,\mu$s for all channels.

For the end mirror channels in LN mode, the delays are compatible with the expected ones within $5\,\mu$s. The delay in HP mode is $\sim 66\,\mu$s higher than in LN mode as expected from the different serie resistors.

For the BS mirror channels in LN mode, differences of $\sim 40\,\mu$s are found between the up and the down channels. The DL and DR channels have a delay in HP mode $\sim 66\,\mu$s higher than in LN mode as expected, while it is $\sim 90\,\mu$s for the UL and UR channels.

To conclude, **the measured actuation delay in LN mode is compatible within $5\,\mu$s with the expected delay for the end mirrors and different by $\pm 20\,\mu$s for the BS**

[7] The equivalent delay due to the 3-97 Hz shaping filter is 59, 14.9 and 3.7 μs at 500 Hz, 1 kHz and 2 kHz respectively.

mirror with difference between the different channels. Since the origin of the BS difference is not understood, it could be in the actuation chain itself and not in the readout part of the $Ca\_*\_RM\_Coil*$ channels. These numbers are thus an upper value of the systematic errors on the actuation timing.

5.2 Propagation of the mirror deformation to the mirror center

The actuation force is applied on the mirror at the level of the magnets. The mirror deformation then propagates to the center of the mirror at the speed of sound. The mirror motion is seen in the interferometer when the deformation reaches the main laser beam, at the center of the mirror. The beam radius being of the order of 3 cm, the deformation reaches the beam before the center of the mirror, reducing this delay.

The relevant characteristics of the mirrors [3] concerning the propagation of sound waves are given in the table 5. The speed of acoustic waves in silica is $5968\,\mathrm{m.s^{-1}}$ for longitudinal waves and $3764\,\mathrm{m.s^{-1}}$ for transverse waves. The propagation times of the mirror deformation from the magnet position to the center of the interferomater beam have been estimated for both types of waves in the table 5. The expected delays must be between the two estimated delays.

Some arguments against such a delay have been highlighted in LIGO-Virgo calibration meetings. The idea was that the summation of all the waves might interfere and build a standing wave, inducing no delay from deformation propagation. This is not clear yet and finite element analysis are underway in order to understand how to take it into account.

	BS	NI, WI	NE, WE
Material	SUPRASIL 311	SUPRASIL 312	HERASIL 1
Thickness e (mm)	55.0	96.8	95.7
Diameter D (mm)	230	350	350
Magnet position diameter d (mm)	215	305	305
Magnet position face	reflective (west)	non-reflective (back)	non-reflective (back)
Propagation time (μs)			
Longitudinal waves	18	30	30
Transverse waves	29	48	48

Table 5: ***Mirror characteristics, magnet positions and delays for deformation propagation.*** *The expected delays from the position of the magnets to the center of the mirror are given for longitudinal and transverse waves.*

5.3 Optical response of the interferometer

Two configurations with different time of light travel in the arms have to be considered.

The measurements of the delay from Sc_ ∗ _zCorr to Pr_B1_ACp are based on data in **free swinging Michelson** configurations. In these configurations, the light directly travels from the mirror to the dark fringe. The expected delay is thus 10 μs from the end mirror to the dark fringe photodiodes ($\sim$ 3 km), and negligible from the input mirrors. These delays appear in the overall Sc_ ∗ _zCorr to Pr_B1_ACp delay measured in the main stream calibration.

For the BS mirror, different cases have to be taken into account as described in the note **??**: the path from the BS to the dark fringe can be delayed by 20 μs for the beam going to the WE mirror, while there is no delay for the beam going to WI or coming from the north cavity. This delay has been corrected for in the calibration main stream such that the quoted delays assume no propagation delay.

In **Science Mode**, the ligth is stored in the Fabry-Perot cavities, with a finesse of $\sim$ 50. The optical response for the signals from the end mirror to the dark fringe photodidoes is modeled by a simple pole with a pole of $\sim$ 500 Hz. For frequencies lower than 500 Hz, the phase is equivalent to a delay of the order of 320 μs. The pole of the cavities is taken into account in the h-reconstruction. No delay from the optical response of the interferometer should thus be taken into account in the overall Sc_ ∗ _zCorr to Pr_B1_ACp delay added in the h-reconstruction.

5.4 Dark fringe sensing timing

The signal processing, expected delays and measurements have been described in 4 for the channel Pr_B1_ACp. The expected delay, from the ADC anti-alias filter, is in the range $70 - 80\,\mu$s. The measurements of the dark fringe readout electronics have shown that the two photodiode channels have delays of 72.8 and 79.7 μs respectively. Using an average filter (Butterworth, notch and delay) for both channels would thus induce $\pm 4\,\mu$s systematic errors on the timing of the combined channel.

Concerning the channel Pr_B1p_ACp that was used to compute the transfer function from actuation to dark fringe using free swinging Michelson data in the main stream calibration, no measurements are available.

TO DO: TF B1/B1p during VSR1

5.5 Summary

The summary of the expected delay from Sc_ $*$ _zCorr to Pr_B1_ACp for the end mirrors is shown in the figure 11 in the case of free Michelson data in LN mode. The expected delay for free Michelson data in LN mode are summarized in the table 6 and compared to the delay measured from the calibration main stream.

Note that the delay from the sensing described in this note is based on measurements of the Pr_B1 photodiodes while the averall delay measured from the calibration main stream are based on free Michelson data using the Pr_B1p photodiodes.

For the end mirrors, the measured delay is compatible with the expected one. It is also the case at the level of the coil actuation part.

For the BS mirror, the measured delay is $\sim 37\,\mu$s lower than expected. Large discrepancies, up to $\sim 40\,\mu$s, have also been measured in the coil actuation part between the UL-UR and DL-DR channels respectively. It must indicate a problem in the UL and UR channels in LN mode where the expected delay is $\sim 30\,\mu$s lower than expected.

Such differences can be used as a systematic error in the delay measurements.

Delay origin	From NE, WE		From BS	
	Expected	Measured	Expected	Measured
Coil actuation	331	325 ± 4	333	$307 - 347$
Mirror deformation	39 ± 9	-	22 ± 5	-
Light propagation	10	-	0	-
Dark fringe sensing	75 ± 5	76 ± 4	75 ± 5	76 ± 4
Total delay	455 ± 14	451 ± 1	430 ± 10	393 ± 1

Table 6: ***Summary of the expected delays (in μs) from the mirror actuation (LN mode) to the dark fringe readout*** *in free swinging Michelson configurations. The corresponding delay measured in the calibration main stream is also given for comparison.*

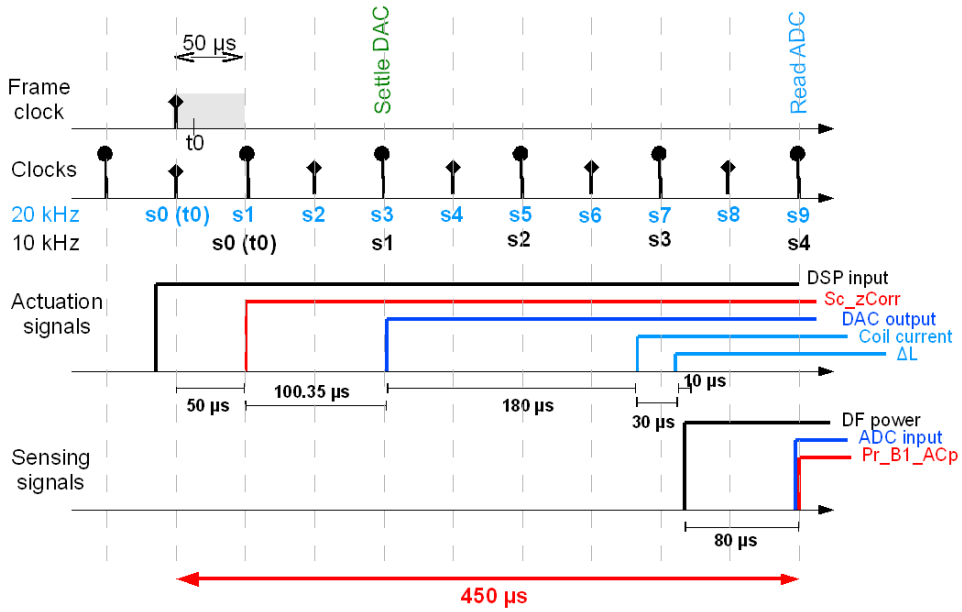

Figure 11: ***Signal processing from*** Sc_ ∗ _zCorr ***to*** Pr_B1_ACp ***for the end mirrors in LN mode.*** *The model for the optical corresponds to data in free swinging Michelson configuration.*

6 Checks of the Virgo timing system stability

6.1 Timing jitter

A spectrum of the jitter of the timing system has been measured in April 2008 (see logbook entries 20292 and 20293). The 10 MHz signal from the atomic clock is used as a reference signal that is compared to one of the signals used by the timing system, the 2.5 MHz so called *fast clock* signal.

A first measurement of the signal using an oscilloscope shows an RMS of about 200 ns (integrated over many seconds). This is consistent with the observed RMS of $\sim$ 200 ns for the propagation time to each building measured using two different GPS receivers (the TiM_rtt$\{1,2,3,4\}$ signals), measurement limited by the 100 ns resolution of the GPS receivers.

The comparison of the signals produced simultaneously by two timing boards, or by the propagation trough 3 km of optical fibers gives an RMS less than 0.2 ns. This means that the jitter introduced by the timing distribution is much smaller than the one of the GPS receiver.

To get a spectrum of the overall timing jitter and therefore validate this hypothesis, the 2.5 MHz signal was mixed with the 10 MHz signal using a demodulation board (B1_d7) and acquired in phase and quadrature (the compression filters have been compensated for). The phase and quadrature signal gives a measurement of the relative dephasing of the two signals at 10 MHz. Integrating this phase, the time difference between the two clocks, and therefore the jitter of the timing distribution, can be reconstructed.

The figure 12 shows the spectrum of this signal. Above one 1 Hz, the estimated time jitter is below 1 ns/$\sqrt{\text{Hz}}$. At low frequency there is a bump corresponding to the 200 ns previously observed RMS.

6.2 Absolute time variations during VSR1

The monitoring signals TiM_GTimeN and TiM_rtt$\{1,2,3,4\}$ of the timing system during VSR1 are shown in figure 3.

The delay between the master timing clocks and the GPS receiver clock changed from 2.7 to 2.3 μs on August 3rd 2007, around 14h18m42s UTC.

The RMS of the TiM_rtt$\{1,2,3,4\}$ during VSR1 are of the order of 200 ns, negligible compared to the propagation delay of 34.1 μs.

An independent atomic clock is used to check that there is no glitches in the Virgo timing system. The 1 PPS signal from the atomic clock is converted into a ramp (as described in 3.1.2 (p. 5)), sampled through a 16-channels ADC and stored in the DAQ. A fit of the ramp is performed online in order to estimate the delay between the 1 PPS and the frame clock. The delay is saved in the channel TiMoni_Ti_AtomicPulse_t0 in secondes. Its evolution during VSR1 is shown in the figure 13(a). The atomic clock is more stable than the clock from the GPS receiver at short term, but derives at longer term compared to the reference GPS time.

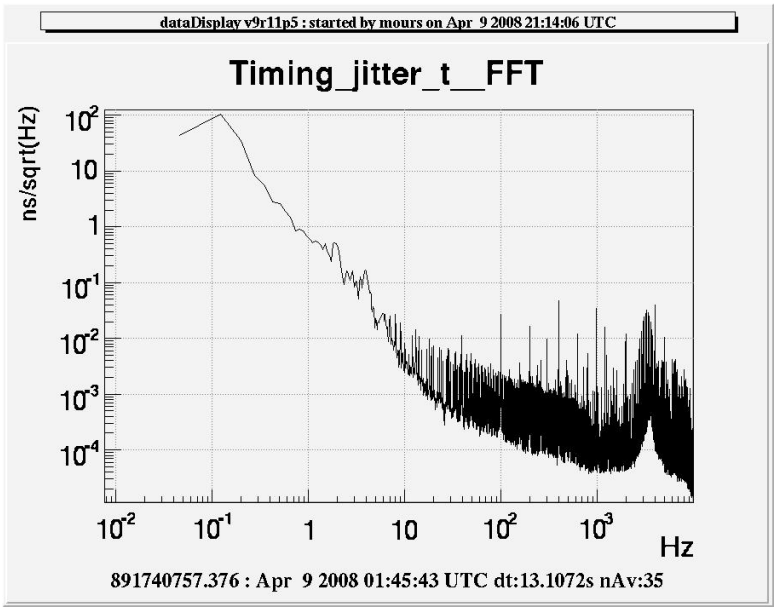

Figure 12: ***Spectrum of the jitter of the timing system.***

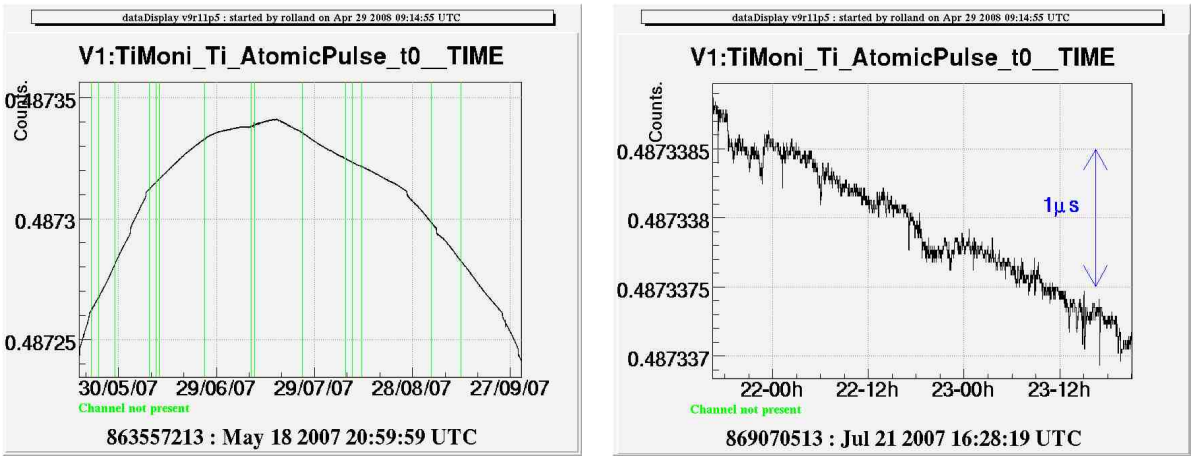

(a) VSR1 monitoring.

(b) 2 days monitoring.

Figure 13: ***Monitoring of the channel*** TiMoni_Ti_AtomicPulse$_t$0 ***during VSR1 and estimation of the signal width.***

An estimation of the short term error of the Virgo timing system is given by the width of the signal corrected for the long term deviation. The error can be estimated from figure 13(b) to be less than 1 μs.

7 Conclusions

The absolute timing of the Virgo data have been measured. During VSR1, a delay of 21 μs have been estimated for the dark fringe signal time-serie, with a systematic error of 2 μs. The Virgo time jitter has been estimated to be lower than 200 ns.

The two photodiode readout channels that are used to compute the dark fringe channel Pr_B1_ACp have been characterized up to $\sim$ 10 kHz. An additionnal systematic error of 4 μs on the Pr_B1_ACp timing has to be added since the measured delays are different between the two channels.

The delay from the Sc_ $*$ _zCorr channels in LN mode to the dark fringe channel Pr_B1_ACp has been estimated from the different pieces of the chain. They are in agreement with the delays measured by the calibration main stream within 6 μs for the end mirror actuation. A difference of 37 μs is observed for the BS mirror actuation. The difference might come from a problem in the UL and UR channels of the BS but is not understood yet. This gives the order of the tuning of the delays that could be done to combine the actuation signals and the dark fringe signal in the h-reconstruction. It includes the 4 μs error on the dark fringe channel found above.

In conclusion, the systematic errors of the dark fringe absolute timing, after correction of the Virgo absolute time offset, are estimated to the order of 6.5 μs. The systematic errors on the mirror actuation timing that is important to combine the correction signals and the dark fringe signal in the h-reconstruction below a few 100's Hz, are estimated to 10 μs for the end mirrors and 40 μs for the BS mirror.

References

[1] A. Masserot et al. (VIRGO collaboration), *The Virgo Data Acquisition System* (2003) Proc. of the 13th IEEE NPSS Real Time Conference, Montreal, Canada (Virgo note LAPP-EXP-2003-12).

[2] L. Rolland, F. Marion, B. Mours *Mirror and marionette actuation calibration for VSR1* (2008) VIR-015A-08.

[3] P. Puppo, *A finite element model of the Virgo mirrors* (2004) VIR-NOT-ROM-1390-262.